RESEARCH ARTICLE

Key Points:
- A new determination of the boundary for ULF waves in the Earth foreshock
- A specific, accurate, and robust criterion for crossings determination is present
- The boundary is compared with previous results and theoretical predictions

Correspondence to:
N. Andrés,
nandres@iafe.uba.ar

The ULF wave foreshock boundary: Cluster observations

Nahuel Andrés[1,2], Karim Meziane[3], Christian Mazelle[4], Cesar Bertucci[1,2], and Daniel Gómez[1,2]

[1]Instituto de Astronomía y Física del Espacio (CONICET-UBA), Buenos Aires, Argentina, [2]Departamento de Física (FCEN, UBA), Buenos Aires, Argentina, [3]Physics Department, University of New Brunswick, Fredericton, New Brunswick, Canada, [4]Institut de Recherche en Astrophysique et Planétologie, Toulouse, France

Abstract The interaction of backstreaming ions with the incoming solar wind in the upstream region of the bow shock gives rise to a number of plasma instabilities from which ultralow frequency (ULF) waves can grow. Because of their finite growth rate, the ULF waves are spatially localized in the foreshock region. Previous studies have reported observational evidence of the existence of a ULF wave foreshock boundary, whose geometrical characteristics are very sensitive to the interplanetary magnetic field (IMF) cone angle. The statistical properties of the ULF wave foreshock boundary (UWFB) are examined in detail using Cluster data. A new identification of the UWFB is presented using a specific and accurate criterion for identification of boundary crossings. This criterion is based on the degree of IMF rotation as Cluster crosses the boundary. The obtained UWFB is compared with previous results reported in the literature as well as with theoretical predictions. Also, we examined the possible connection between the foreshock boundary properties and the ion emission mechanisms at the bow shock.

1. Introduction

The upstream region magnetically connected to the bow shock is known as the foreshock. This region is populated by a small fraction of the incoming solar wind particles which are reflected at different locations of the bow shock back into the solar wind. These backstreaming particles are subjected to the solar wind's $\mathbf{E} \times \mathbf{B}$ drift, where $\mathbf{E} = -\mathbf{v}_{sw} \times \mathbf{B}$, is the solar wind's convective electric field, $\mathbf{B}$ is the interplanetary magnetic field (IMF), and $\mathbf{v}_{sw}$ is the solar wind velocity. As a result, the guiding centers of all backstreaming particles move within the $\mathbf{v}_{sw} - \mathbf{B}$ plane, gradually drifting away from the field line tangent to the bow shock toward the inner part of the foreshock and being segregated according to their parallel velocities. Backstreaming ions can drive a number of plasma instabilities [e.g., *Gary*, 1993], leading to the generation of ultralow frequency (ULF) waves. The ion foreshock is then characterized not only by the presence of backstreaming ions but also by the generation and propagation of plasma waves around the local ion cyclotron frequency.

An early study based on Vela measurements reported by *Asbridge et al.* [1968] showed that a fraction of ions from the solar wind are often accelerated at the Earth's bow shock and reflected into the solar wind. Using Explorer 43 data, *Lin et al.* [1974] presented evidence of backstreaming protons in the 30–100 keV range whose presence was attributed to the interaction between 3 and 4 keV reflected protons and Alfvén waves. Observations made by the dual spacecraft ISEE allowed for the identification of different types of backstreaming ion distributions at the Earth's foreshock: reflected ions (now called field-aligned beams), intermediate, and diffuse distributions [*Gosling et al.*, 1978; *Paschmann et al.*, 1981; *Thomsen et al.*, 1985]. This classification of backstreaming ion populations was made on the basis of two-dimensional velocity distribution functions and energy-time spectrograms. Further results from ISEE demonstrated the existence of gyrophase-bunched and gyrotropic backstreaming ion distributions in the foreshock [*Gurgiolo et al.*, 1983]. These gyrating ion distributions are characterized by a gyromotion around the magnetic field, i.e., a nonvanishing perpendicular bulk velocity with respect to the background magnetic field [*Thomsen et al.*, 1985; *Fuselier et al.*, 1986a, 1986b; *Fuselier*, 1994; *Fazakerley et al.*, 1995; *Meziane et al.*, 1997, 2001; *Mazelle et al.*, 2003].

The field-aligned beam (FAB) distributions populate a region located just downstream from the ion foreshock boundary. This distribution originates from the quasi-perpendicular sector of the bow shock, i.e., $\theta_{Bn} > 45°$, where θ_{Bn} is the angle between the IMF and the local normal to the shock. As a result, the FAB region displays an inner and an outer boundary. Within this region no ULF waves are observed [*Paschmann et al.*, 1979]. These ions are characterized by a bulk motion essentially along the IMF of the order of a few v_{sw} (in the plasma reference frame) and a velocity spread of a few hundreds of km s^{-1} [*Meziane et al.*, 2013]. Basic production

mechanisms for the FABs have been investigated elsewhere [e.g., *Thomsen et al.*, 1983a]. *Kucharek et al.* [2004] using Cluster multispacecraft measurements showed that the FABs result from effective scattering in pitch angle during reflection in the shock ramp [see also *Miao et al.*, 2009]. However, a comprehensive understanding of FAB production mechanisms still needs clarification. Downstream from the FAB region, gyrating ion distributions are often detected in association with quasi-monochromatic ULF waves with substantial amplitudes, i.e., $\delta \mathbf{B}/B \sim 1$ [*Mazelle et al.*, 2003]. The gyrating ion distributions could be nongyrotropic, i.e., gyrophase bunched, or nearly gyrotropic. There are mainly two possible mechanisms for the origin of gyrating ion distributions, the waves (produced through a beam plasma instability) trap the ions and cause the phase-bunched distribution [*Hoshino and Terasawa*, 1985; *Mazelle et al.*, 2000; *Meziane et al.*, 2001; *Mazelle et al.*, 2003], or a portion of the incoming solar wind is specularly reflected at the bow shock [*Gurgiolo et al.*, 1983; *Gosling et al.*, 1982; *Meziane et al.*, 2004a]. *Möbius et al.* [2001] studied the spatial and temporal structure of FAB and gyrating ring distributions at the quasi-perpendicular bow shock with Cluster Ion Spectrometry (CIS) data. *Schöler et al.* [2000] provided a theoretical background. These authors suggest a common origin of ring and beam populations at quasi-perpendicular shocks in the form of specular reflection and immediate pitch angle scattering. Using a 2-D particle-in-cell (PIC) code, *Savoini et al.* [2013] analyzed the ion foreshock for quasi-perpendicular conditions. Their numerical results suggest that FABs and gyrating ion distributions can be produced from different interactions with the shock front without the need of any pitch angle scattering induced by wave-particle interaction. Finally, diffuse ion distributions spread out a shell of nearly constant radius about a mean velocity field. The bulk velocity of diffuse ions is approximately v_{sw} (in the plasma reference frame) and are found even farther away from the ion foreshock boundary in quasi-parallel shock regions, i.e., $\theta_{Bn} < 45°$ [*Bonifazi and Moreno*, 1981a]. Possible mechanisms of generation of diffuse ion distributions can be found elsewhere [*Sarris et al.*, 1987; *Gosling et al.*, 1989; *Jones and Ellison*, 1991]. Diffuse distributions are in fact observed in the presence of nonlinear, steepened ULF waves [*Paschmann et al.*, 1979, 1981; *Hoppe et al.*, 1981] and associated with quasi-parallel shock processes [*Gosling et al.*, 1989].

The most frequent type of ULF waves observed in the Earth's ion foreshock are large amplitude waves with periods from about 20 to 40 s, the so-called "30 s" waves. Their waveforms vary from quasi-monochromatic, coherent and transverse to the ambient magnetic field to highly compressional and steepened (the so-called *shocklets*) [*Hoppe et al.*, 1981; *Le and Russell*, 1992a; *Greenstadt et al.*, 1995; *Lucek et al.*, 2002; *Eastwood et al.*, 2005; *Burgess et al.*, 2005]. The quasi-monochromatic 30 s waves are usually observed with a left-handed polarization in the spacecraft frame [*Fairfield*, 1969]. However, this kind of waves is intrinsically right handed and propagate against the solar wind flow [*Hoppe et al.*, 1981]. Theoretical works has established that 30 s waves are generated via the ion-ion right-hand resonant beam instability [*Gary*, 1991; *Convery and Gary*, 1997]. Using Cluster data, *Mazelle et al.* [2003] were the first to firmly prove this theoretical prediction from observations. Intrinsically left-handed and sunward propagating ULF waves have also been observed in the foreshock [*Eastwood et al.*, 2003]. The excitation source of these waves is still unknown.

The region of ULF wave activity is embedded in the ion foreshock. Because of the finite growth rate of effective instabilities combined with convection, these waves reach significant amplitudes away from the source region. Therefore, for quasi-stable IMF directions, the onset of waves is spatially localized in an extended surface in the ion foreshock known as the ULF wave foreshock boundary (UWFB). For a precise identification of the UWFB, the mean magnetic field is expected to perform a very slow and monotonic rotation as the spacecraft crosses this boundary. This is a central point of the boundary morphology as the UWFB orientation depends on the IMF direction. The onset of waves in coincidence with large IMF rotations would be in conflict with the quasi-steadiness condition and therefore might lead to an incorrect identification of the boundary. An early study on the UWFB by *Diodato et al.* [1976] using magnetic field data from Heos-1 shows that the boundary is strongly dependent upon the cone angle θ_{Bx}, the angle between the IMF direction and the $\hat{\mathbf{x}}_{gse}$ axis. However, the low-resolution magnetic data (48 s) used in this work-induced significant uncertainties on the boundary crossings. A decade later, using ISEE 1 data, *Greenstadt and Baum* [1986] (GB86) confirmed *Diodato et al.*, 1976's 1976 results. Even though the time resolution of magnetic field data was better, no quantitative criteria for the identification of boundary crossings was considered by GB86. As a result, their identification of the UWFB may have included crossings with large IMF rotations. Although the authors used the ULF waves onset as a qualitative criterion for boundary crossing identification, they did not include any quantitative limit on the amplitude of the fluctuations. In another study based on magnetometer data from ISEE 1 and 2, *Le and Russell* [1992b] examined 373 bow shock outbound crossings and recorded whether or not ULF fluctuations are present immediately upstream. They found that ULF waves are present only for θ_{Bn} less than ~50°. Given
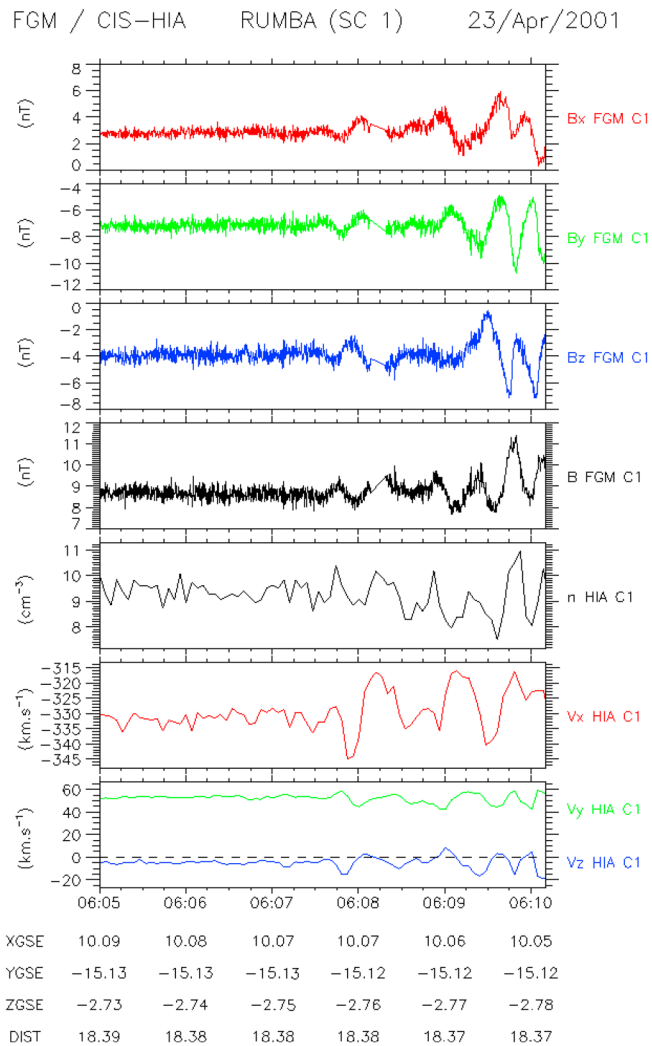
Figure 1. A UWFB crossing made by Cluster on 23 April 2001. Cluster is entering the ULF wave region with $\alpha = 2° \pm 1°$.

the association of foreshock particle distributions with the ULF waves, *Meziane and D'Uston* [1998] (MD98) presented a statistical investigation of the location of the onset of intermediate and gyrating ion populations in the Earth foreshock based on the Fixed Voltage Analyzer data from ISEE 1. They found that for $\theta_{Bx} = 45°$, the spatial location for intermediate ions coincides with the UWFB reported by GB86. To locate the ion boundary crossings, the authors adopted a measurable criterion based on an intermediate flux level between the background level in the interplanetary medium and the higher level of ion flux events. Nevertheless, they did not establish any criterion based on the magnetic field fluctuations or rotations. A more recent study based on Cluster data, *Meziane et al.* [2004b] reported for the first time FABs and gyrating ion distributions which are observed simultaneously. The authors suggested that Cluster spacecraft might be traveling tangentially to the boundary between these two populations.

Theoretical investigations on the ULF foreshock boundary are noticeably few. To the best of our knowledge, *Skadron et al.* [1988] is the only self-consistent spatiotemporal study involving the interaction between energetic protons backstreaming pre-existing and hydromagnetic waves in the Earth's ion foreshock in a theoretical frame. Using a parabolic fit to the bow shock, they found the boundary for the region of compressional waves (corresponding to different IMF orientations) using a criterion based on the compressional component of the magnetic fluctuations, $\delta|\mathbf{B}|$. The authors define a theoretical wave compressional boundary where $\delta|\mathbf{B}|$ becomes larger than its value in the solar wind (1.32×10^{-2} nT, according to equation (29) in the text). For a cone angle $\theta_{Bx} = 45°$, *Skadron et al.* [1988] found that the compressional boundary makes an angle $\zeta = 78°$ with the Earth-Sun axis.

A comparison of the studies summarized above reveals significant discrepancies in the location of the UWFB. The lack of a common criterion for a boundary crossing certainly constitutes the main reason. The aim of the present work is to investigate the UWFB using a quantitative criterion based on magnetic field measurements with a suitable time resolution for ULF wave detection. This determination will require a stationary condition for the magnetic field direction, which will be discussed in the following sections. A precise determination of the UWFB puts strong constraints on models involving wave-particle interactions occurring upstream of the bow shock, and at the same time it sheds light on the particle emission mechanisms at the Earth bow shock.

In situ observations made by the flux gate magnetometer (FGM) and the Cluster Ion Spectrometer (CIS) are presented in section 2. Observations of ULF boundary crossings are presented in section 3. After, we introduce the Solar Foreshock system of coordinates in section 4; the statistical results are presented in section 5. An
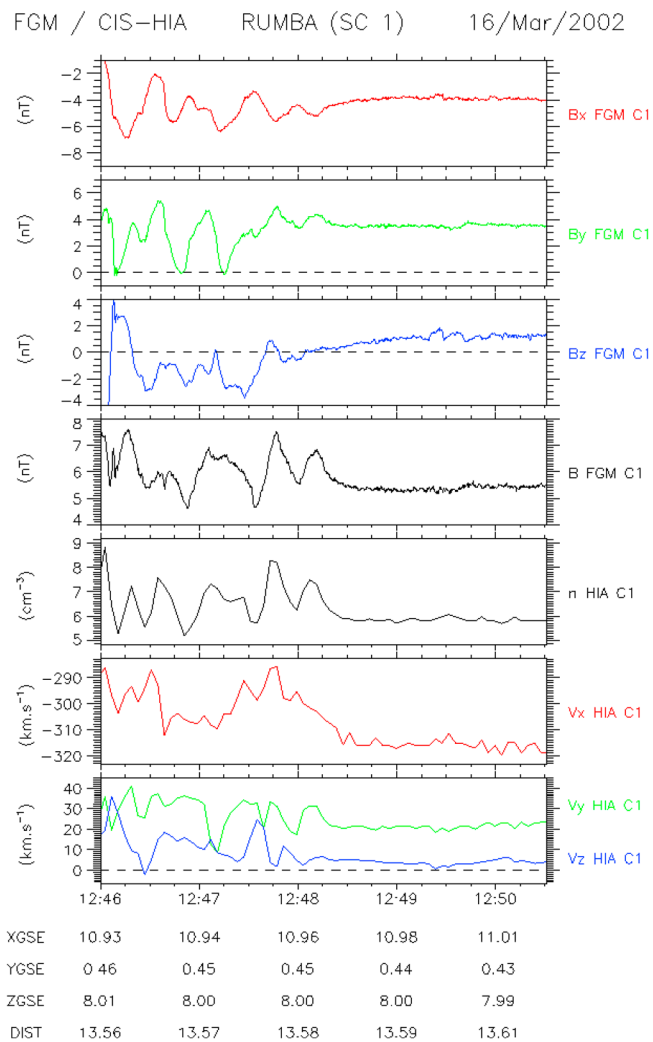
Figure 2. A ULF wave region crossing (ending) made by Cluster on 16 March 2002. In this case, $\alpha = 24° \pm 1°$.

attempt of an interpretation of the data is presented in section 6 followed by a short conclusion in section 7.

2. Data Measurements

The observations used for the present paper consist of magnetic field and solar wind velocity vectors and plasma density measured by Cluster spacecraft obtained upstream from the Earth bow shock during the first three years of Cluster's orbital data, i.e., from February 2001 to December 2003.

We have used a cadence of 5 s^{-1} of magnetic field data from the flux gate magnetometer (FGM) onboard Cluster to investigate the presence of ULF waves upstream from the Earth bow shock. The particle data used in the present study are from the Cluster Ion Spectrometer (CIS) experiment, which includes a top-hat electrostatic analyzer (HIA) and a mass spectrometer (CODIF), which combines a top-hat electrostatic analyzer with a time-of-flight section to measure the major species, i.e., H$^+$, He$^+$, He^{++}, and O$^+$ over an energy range 0.02–38 keV/q. The HIA detector operates according to several modes. The velocity distributions are obtained from both instruments, which accumulate full 3-D distribution functions within one spin period (4 s), with an angular resolution of 22.5° × 22.5°. For

a more extensive description of FGM and CIS/CODIF Cluster experiments see *Balogh et al.* [1997] and [*Rème et al.*, 2001], respectively. If a boundary crossing occurs when the HIA instrument is not operating in the solar wind mode, the plasma measurements from Cluster-CIS are not reliable. In this case, we estimated the solar wind density and velocity from plasma data taken by WIND/3DP experiment. For some events, the WIND spacecraft is located upstream as far as ∼250 R_E, and therefore, for these cases a time delay between WIND and Cluster spacecraft was taken into account.

3. Identification of UWFB Crossings

During Cluster excursions into the solar wind, we looked for intervals displaying patterns of ULF waves in the magnetic field components. For the determination of these crossings, we made no distinction regarding the type of magnetic field fluctuations, requiring only that the transition from (or to) the wave region would be clearly apparent. For each identified crossing, we extracted **B**, $\mathbf{v}_{sw}$ and n_{sw} data from the Cluster Active Archive and the CLWeb data base (http://clweb.cesr.fr/). The ULF wave foreshock boundary (UWFB) is a surface embedded in the foreshock region. By definition, the region *downstream* from the UWFB is the one that displays ULF wave activity, while the region *upstream* does not. For the purpose of the present study, we find that the optimal time interval to compute mean values of the quantities listed above lies between three and six wave periods at each side of the boundary. We reached this conclusion after following this procedure: for a test set of 10 crossings with particularly long and quasi-monochromatic wave activity (10 periods or more)
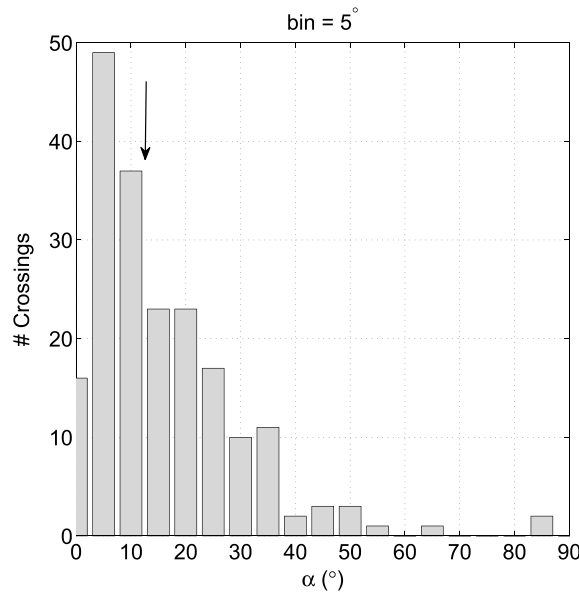
Figure 3. Histogram of α for the 192 identified crossings. The arrow is located at $\alpha = 12.5°$, which is the upper limit adopted for the stationary UWFB.

downstream from the boundary we computed the mean values of the magnetic field components for progressively shorter time intervals. We find that for time intervals of between three and six wave periods, the mean value remains within 1 standard deviation from the longer average and it is therefore sufficiently long to be representative of the mean magnetic field in that region.

The UWFB can be observed only under quasi-stationary IMF conditions, i.e., the mean solar wind magnetic field has to remain quasi-stationary as Cluster crosses the boundary. The foreshock geometry critically depends on the IMF direction. In particular, as Cluster crosses the boundary between the upstream and the downstream region, we invariably observe a rotation of the IMF. Therefore, if we define the angle α as,

$$\cos \alpha \equiv \frac{\mathbf{B}_{up} \cdot \mathbf{B}_{dw}}{B_{up} B_{dw}} \tag{1}$$

it is possible to quantitatively analyze the degree of IMF rotation as Cluster passes from the upstream to the downstream region. In equation (1), $\mathbf{B}_{up}$ ($\mathbf{B}_{dw}$) is the mean magnetic field in the upstream (downstream) region, meanwhile B_{up} (B_{dw}) corresponds to its absolute value. Then, as long as α remains small we are able to investigate the quasi-stationary scenario and consequently the UWFB. Figure 1 shows an example of Cluster entering to the wave region on 2001 April 23 at 0607:24 UT in which $\alpha = 2° \pm 1°$ (note that there is a small FGM data gap at 0608:15 UT in Figure 1 (first to fourth panels)). In contrast, Figure 2 shows an example of Cluster leaving the wave region on 16 March 2002 at 1248:17 UT with $\alpha = 24° \pm 1°$.
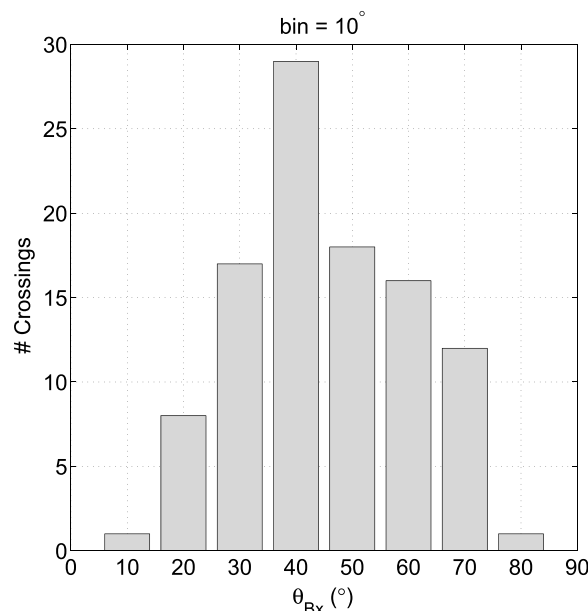
From February 2001 through December 2003, we have identified 192 ULF wave/no wave transitions. Figure 3 shows a distribution of these transitions with respect to the α angle. As it can be seen, the histogram displays a strong peak at small values of α, in particular for the most frequently value at 5°. The histogram corresponds to a nonsymmetric and positively skewed distribution. Fifty percent of the crossings occur for $\alpha < 12°$ (i.e., 12° corresponds to the median value of the distribution) and 78% of the events occur for angles less than the mean value of 16°. For a better determination of the boundary location, only wave crossings with $\alpha < 12.5°$ (black arrow in Figure 3) were considered, which includes 102 events. As we

Figure 4. Histogram of the cone angle θ_{Bx} for the 102 identified crossings with $\alpha < 12.5°$ correspond to the upstream region.

discussed in section 1, the UWFB is defined for a given IMF orientation. Figure 4 shows the cone angle (θ_{Bx}) distribution corresponding to these 102 events. There is no indication that boundary crossings occur for a particular IMF direction other than the Parker's prediction, since the distribution is consistent with the IMF spiral orientation at 1 AU. Following previous studies, results of our statistical survey is performed using 10° bins for the θ_{Bx}.

In a previous study, [*Andrés et al.*, 2013] presented a different approach to the determination of the UWFB crossings at Saturn. The authors considered a quasi-stationary crossing according to the following criterion: for each component of the magnetic field ($j = x, y, z$) if the difference between the average values in the upstream region ($B_{up,j}$) and in the downstream region ($B_{dw,j}$) is smaller than the standard deviation in the upstream region ($\sigma_{dw,j}$), they consider that the spacecraft crossed a quasi-stationary UWFB,

$$|B_{up,j} - B_{dw,j}| < \sigma_{dw,j} \quad \text{for} \quad j = x, y, z \tag{2}$$

Following the same criterion established by *Andrés et al.* [2013], we found that 127 of the 192 crossings correspond to quasi-stationary crossings. In this sense, we conclude that the current criterion based on the IMF rotation is more restrictive than the criterion used by *Andrés et al.* [2013].

For our analysis, the criterion based on the magnitude ($\alpha < 12.5°$) level of IMF rotation is used to identify a UWFB crossing. The determination of the UWFB spatial location requires to know the position of the Earth's bow shock. For this purpose, we use the *Farris et al.* [1991] (F91) gas dynamics bow shock model.

4. Solar Foreshock Coordinates

In order to identify the UWFB independently from the changes in the IMF or the location of the bow shock, we employed the so-called solar foreshock coordinates (SFC) introduced by GB86. First, we construct the foreshock geometry based on the F91 bow shock model. In this model, the bow shock location and shape are defined by the solar wind ram pressure. The bow shock model is axially symmetric about the Earth-Sun direction and has the following functional form

$$r = \frac{L}{1 + e\cos\theta} \tag{3}$$

where r is the distance from the planet to a point on the shock surface, θ is the corresponding polar coordinate angle with respect to the symmetry axis, L is the semilatus rectum (size parameter) and e is the eccentricity. To rescale the size parameter L, we used the fact that the location of the bow shock varies as the inverse one-sixth power of the dynamic pressure [*Binsack and Vasyliunas*, 1968],

$$L = \left(\frac{p}{p_0}\right)^{-\frac{1}{6}} L_0 \tag{4}$$

where p is the ram pressure and p_0 is a reference ram pressure. The F91 model uses a fixed eccentricity $e = 0.81 \pm 0.02$ (ellipsoidal model), a nominal parameter size $L_0 = (24.8 \pm 0.2)R_E$ with a reference ram pressure $p_0 = 1.8$ nPa and a nominal zero focus position. In contrast to hyperbolic models, the F91 elliptic model has not a flaring angle. F91 provides a statistical model for the shape of the Earth's bow shock. There are numerous bow shock models available in the literature and their reliability is parameter-dependent [*Merka et al.*, 2005]. Our choice [*Farris et al.*, 1991] is dictated by its simplicity since it is only solar wind ram pressure dependent. It is clear from equations (4) that in situ solar wind density and velocity measurements are necessary to accurately determine the location and shape of the bow shock.

In the SFC coordinate system, the $\hat{\mathbf{x}}$ axis points toward the Sun (it is parallel to $\hat{\mathbf{x}}_{gse}$), and the $\hat{\mathbf{x}} - \hat{\mathbf{y}}$ plane is the $\mathbf{v}_{sw} - \mathbf{B}$ plane which contains the location of the spacecraft at a given quasi-stationary crossing of the UWFB. The position of each boundary crossing is fixed by calculating the SFC coordinates μ and ν (see Figure 5).

$$\mu = \frac{(y_o - y_t)}{\sin\theta_{Bx}}$$

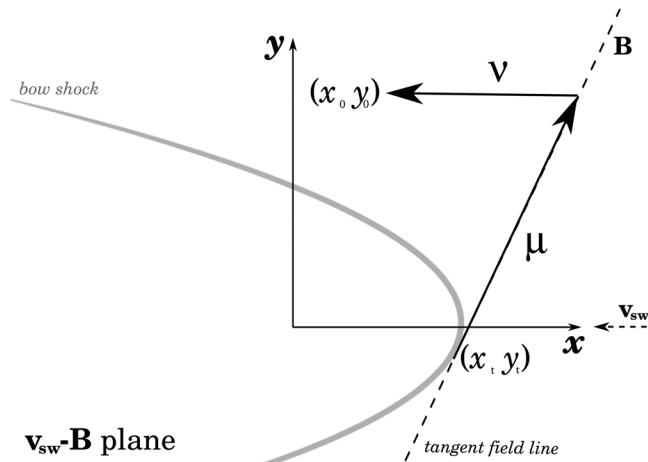$$\nu = \frac{(y_o - y_t)}{\tan\theta_{Bx}} + x_t - x_o \tag{5}$$

Figure 5. Schematic representation of the Solar Foreshock Coordinates (SFC).

where θ_{Bx} is the IMF cone angle, (x_t, y_t) and (x_o, y_o) are the IMF line tangent point to the bow shock model and the observation point respectively. The coordinate μ is the distance along the tangent magnetic field line between the tangent point and the observation point. The coordinate ν is the distance along the $\hat{x}_{gse}$ direction between the tangent magnetic field line and the observation point. In this sense, the coordinate ν indicates how far downstream from the IMF tangent line is the UWFB.

5. Statistical Results

Figure 6 shows a scatter plot of the UWFB crossings in SFC for two cases: $20° < \theta_{Bx} < 30°$ (left) and $40° < \theta_{Bx} < 50°$ (right). In these Figures, the best linear fit corresponds to the blue solid line. The uncertainties in the determination of the three magnetic field components, the three solar wind velocity components and the solar wind density are dominated by the statistical error given by the corresponding standard deviation from the mean values. For the determination of the error bars in Figure 6, we propagated these statistical errors. For reference, we included MD98 (dashed red line) and GB86 (dash-dotted line) results. It is worth mentioning the very good agreement between our results and those reported in previous works.

Table 1 shows the parameters of the $\mu-\nu$ regression line ($\nu = p\mu+q$) of the UWFB for different θ_{Bx} ranges, using the F91 bow shock model. For comparison, the results reported by MD98 and GB86 also indicated in the third and fourth column. Except for the range $30° < \theta_{Bx} < 40°$, our determination of the slope of the UWFB line is in good agreement with those obtained by MD98 (when the errors are taken into account). On the other hand, our results for the range $20° < \theta_{Bx} < 30°$ differ significantly from those reported by GB86. Also, based on numerical values listed in Table 1, an increase of the UWFB line slope with θ_{Bx} in the SFC plane cannot be ruled out.
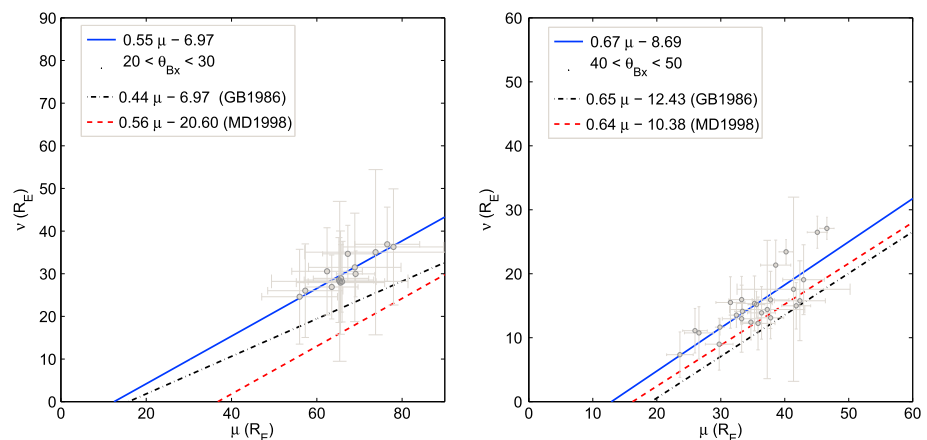

Figure 6. Best linear fit (solid line) of UWFB crossings in SFC, for cone angles $40° < \theta_{Bx} < 50°$ and $20° < \theta_{Bx} < 30°$. For reference, we included MD98 (dashed line) and GB86 (dash-dotted line) results.

Table 1. Parameters of the $\mu-\nu$ Regression Line of the UWFB For Different θ_{Bx} Ranges, Using F91 Bow Shock Model[a]

θ_{Bx} (°)	p	q	r	p_{MD}	q_{MD}	p_{GB}	q_{GB}
20−30	0.56 ± 0.08	-6.97 ± 5.21	0.8937	0.56 ± 0.02	-20.60 ± 2.45	0.44 ± 0.03	-6.97 ± 3.88
30−40	0.55 ± 0.08	-6.43 ± 3.66	0.8510	0.71 ± 0.03	-20.22 ± 1.48	-	-
40−50	0.67 ± 0.09	-8.69 ± 3.48	0.8192	0.64 ± 0.02	-10.38 ± 0.68	0.65 ± 0.04	-12.43 ± 1.56
50−60	0.77 ± 0.10	-10.40 ± 3.14	0.8737	0.66 ± 0.02	-9.23 ± 0.61	-	-
60−70	0.65 ± 0.24	-5.54 ± 6.05	0.6278	0.67 ± 0.03	-8.48 ± 0.64	-	-

[a]The coefficients reported by MD98 and GB86 are included for comparison.

However, the values of q reported in MD98 are in general larger than those obtained in the present study. We suspect that the difference is due to the different bow shock models used in these studies. MD98 used a hyperboloid shape with constant parameters, while in the present work the parameters of the elliptical bow shock are adjusted according to plasma data for each boundary crossing.

6. Physical Implications

One of the most interesting features of the ion foreshock is the interaction of backstreaming ions with the incoming solar wind is the excitation of ULF waves [*Gary*, 1993]. Near the leading edge of the ion foreshock boundary, FABs collimated along IMF lines have been observed upstream from the quasi-perpendicular shocks without the presence of ULF waves [*Paschmann et al.*, 1979]. Deeper into the foreshock region, intermediate, gyrating, and diffuse distributions are usually observed in association with large amplitude ULF waves [*Paschmann et al.*, 1981; *Hoppe et al.*, 1981]. In particular, occurrences of these ULF waves are associated with gyrating ion distributions, while FABs are observed just adjacent to the interval of wave occurrence. Recently, *Meziane et al.* [2004b] reported for the first time a local energetic ion event presenting a clear double-peak spectrum observed by Cluster at approximately $1R_E$ upstream from Earth's bow shock. The lower energy peak was associated with FAB distributions with a steady IMF, while the higher-energy peak was interpreted as gyrating ion distributions having pitch angles of about 30° in association with quasi-monochromatic ULF waves. The authors interpreted the simultaneous observation of the two distinct populations as a UWFB crossing.

In this context and in agreement with *Skadron et al.* [1988], *Meziane et al.* [2004b] reported a boundary between the FAB and the gyrating regions, which forms an angle of $\zeta = 77° \pm 3°$ with respect to the Earth-Sun axis for a single event. As mentioned in section 1, during times when the FABs were observed, the mean magnetic field was steady, while the appearance of the gyrating ion distribution was accompanied by the presence of ULF waves. The authors claim that the changes observed in the proton distributions are likely due to a very weak IMF rotation. However, they did not report explicitly the level of IMF rotation associated with this crossing. *Skadron et al.*'s [1988] compressive criterion is different from the two criteria discussed in this paper (see section 3). Whereas the criterion used in the present study is based on the magnitude of the IMF rotation, *Skadron et al.* [1988] solve for locations where the compressive wave amplitude $\delta|\mathbf{B}|$ rises above its ambient solar wind value. Furthermore, the authors claim that the observed boundary would be farther downstream, where they expect the wave amplitudes to be larger. In the case of $\theta_{Bx} = 45°$, the compressional boundary has a mean inclination of 78° with respect to the Earth-Sun axis which is significantly less than the observed value reported here ($\zeta = 87° \pm 7°$). The difference may be explained by the fact that the observed boundary is based on the wave onset having a larger amplitude than used by *Skadron et al.* [1988], and therefore, the UWFB is expected to be located downstream. Moreover, our results clearly indicate that the slope of the UWFB with respect to the x axis increases with θ_{Bx} angle, which is consistent with the foreshock global structure.

The characterization of the UWFB is an important way of testing the validity of models considering local wave-particle interactions in the foreshock region. The spatial distribution and the dynamics of backstreaming ion distributions in the Earth foreshock has been extensively studied in the literature [*Gosling et al.*, 1978; *Paschmann et al.*, 1981; *Bonifazi and Moreno*, 1981a, 1981b; *Hoppe and Russell*, 1983]. Based on the ratio $P_{gc} = v_{gc}/v_{sw}$ (v_{gc} is the guiding center velocity of backstreaming ions measured in the spacecraft frame and v_{sw} is the solar wind velocity), *Bonifazi and Moreno* [1981a] determined statistical average values $< P_{gc} >$ for different backstreaming ion distributions regardless of the IMF cone angle θ_{Bx}. In particular, the authors find that $< P_{gc} > = 2$ for FAB distributions, $< P_{gc} > = 1.75$ for intermediate distributions, and $< P_{gc} > = 1.18$ for

Table 2. The $\zeta = \tan^{-1}(\frac{\sin \theta_{Bx}}{\cos \theta_{Bx} - p})$ Angle Between the UWFB and the $\hat{x}_{gse}$, the $P = \frac{\tan \zeta}{\tan \zeta \cos \theta_{Bx} - \sin \theta_{Bx}}$ Value, the $P_{gc} = \sqrt{1 + P^2 - 2P \cos \theta_{Bx}}$ Factor, the Angles θ_{Bn} and θ_{Vn}, and the Shock Normalized Velocity in the Plasma Reference Frame $P_s = \frac{\cos \theta_{Vn}}{\cos \theta_{Bn}}$

θ_{Bx} (°)	ζ (°)	P	P_{gc}	θ_{Bn} (°)	θ_{Vn} (°)	P_s
20−30	50.66 ± 0.29	1.78 ± 0.49	0.97 ± 0.01	53 ± 5	28 ± 6	1.46 ± 0.18
30−40	64.86 ± 0.64	1.81 ± 0.41	1.15 ± 0.01	52 ± 3	18 ± 3	1.54 ± 0.10
40−50	86.99 ± 6.00	1.49 ± 0.21	1.05 ± 0.01	47 ± 4	4 ± 3	1.46 ± 0.10
50−60	103.50 ± 2.13	1.29 ± 0.88	1.09 ± 0.01	42 ± 3	14 ± 3	1.30 ± 0.06
60−70	104.10 ± 4.20	1.53 ± 3.50	1.43 ± 0.01	38 ± 7	27 ± 6	1.13 ± 0.12

diffuse distributions. From the histograms reported in the paper [*Bonifazi and Moreno*, 1981a] we estimated a spread of ±0.5 for each $< P_{gc} >$. Considering a fictitious proton beam propagating along the UWFB, MD98 used a straightforward geometric argument to demonstrate that the value of P_{gc} can be, for a fixed θ_{Bx}, related to the boundary parameters. The value of P_{gc} could be interpreted as the bulk ion velocity of ions traveling along the UWFB (normalized to the solar wind speed). Using the same expressions from MD98, as indicated on the caption of Table 2, we found that for $\theta_{Bx} = 45°$, the P_{gc} value associated with the UWFB is 1.05 ± 0.01, in approximate agreement with MD98 findings ($P_{gc} = 1.10 \pm 0.04$). The numerical value of P_{gc} is therefore consistent with the bulk speed of diffuse ions rather than intermediate or gyrating ion distributions. The obtained numerical value for P_{gc} may seem puzzling if we assume that the UWFB corresponds to the waves onset, where one expects the presence of an early phase of a FAB disruption. We emphasize that the large spread (±0.5) in the determination of a particular ion distribution by *Bonifazi and Moreno* [1981a] stems from the fact that they do not consider the IMF cone angle in their classification, which could lead to misinterpret our results. However, this result strongly contrasts with the numerical value associated with the FAB-gyrating boundary $P_{gc} = 1.68 \pm 0.08$ [*Meziane et al.*, 2004b]. Our results also indicate, for $50° \leq \theta_{Bx} \leq 60°$, that the UWFB characteristics seems to be consistent with FAB disruption as wave excitation source, in agreement with the MD98 study.

An interesting aspect of the UWFB is the position with respect to the bow shock, best illustrated with the angles θ_{Bn} and θ_{Vn}. Acceleration models bear a direct relation with the shock geometry. A study based on 373 bow shock crossings from *Le and Russell* [1992b] showed that no ULF waves are present for $\theta_{Bn} \geq 50°$. The straight lines obtained from the best fit of the UWFB are not strictly intercepting the shock. However, given the uncertainties on p and q we were able to construct tangent lines by a rather small translation parallel to the x direction. The obtained values for θ_{Bn} and θ_{Vn} along with their uncertainties are listed on Table 2 for each range in θ_{Bx}. If the uncertainties are taken into account, Table 2 indicates that the UWFB intersects the shock at the transition between quasi-perpendicular and quasi-parallel shock regimes, i.e., $\theta_{Bn} \sim 45°$. For $\theta_{Bx} \geq 40°$, our results are in agreement with *Le and Russell* [1992b] findings. Also, we find that a decrease of θ_{Bn} with increasing θ_{Bx} cannot be ruled out.

Following MD98, we now examine the possible connexion between the UWFB properties and the ion emission mechanisms at the shock. Since the UWFB results from waves excitation generated by shock-accelerated ion beams, a resonant interaction requires a specific beam speed. Briefly, the main shock emission mechanisms are as follows:

1. Magnetosheath particle leakage: *Edmiston et al.* [1982] studied the presence of upstream distributions which have leaked from the magnetosheath conserving their magnetic moment. In order to escape to the upstream region, these magnetosheath particles must at least reach the speed of the bow shock, which can be regarded as a threshold. In particular, this process explains the observation of low-energy ion beams [*Edmiston et al.*, 1982; *Tanaka et al.*, 1983; *Thomsen et al.*, 1983b]. The predicted normalized velocity is

$$P_{m.l.} = P_s = \frac{\cos(\theta_{Vn})}{\cos(\theta_{Bn})} \tag{6}$$

where P_s is the shock velocity or the deHoffman-Teller velocity in the plasma frame of reference normalized to v_{sw}.

Table 3. Predicted Velocities (Normalized to v_{sw}) for the Main Shock Emission Mechanisms, i.e., Magnetosheath Particle Leakage ($P_{m.l.}$), Adiabatic Reflection ($P_{a.r.}$) and Specular Reflection ($P_{s.r.}$)

θ_{Bx} (°)	$P_{m.l.}$	$P_{a.r.}$	$P_{s.r.}$
20–30	1.46 ± 0.18	2.92 ± 0.36	1.06 ± 0.13
30–40	1.54 ± 0.10	3.08 ± 0.20	1.17 ± 0.08
40–50	1.46 ± 0.10	2.92 ± 0.20	1.36 ± 0.10
50–60	1.30 ± 0.06	2.60 ± 0.12	1.44 ± 0.07
60–70	1.13 ± 0.12	2.26 ± 0.24	1.40 ± 0.15

2. Adiabatic reflection: a portion of the solar ions produces an ion beam aligned with the IMF with generally high energies [*Sonnerup*, 1969; *Thomsen et al.*, 1983b]. The reflected ions acquire a speed in the plasma reference frame (normalized to v_{sw}) given by

$$P_{a.r.} = 2P_s \tag{7}$$

3. Specular reflection of a portion of the solar wind ions gives birth to an emission mechanism in the upstream region only when $\theta_{Bn} < 45°$ [*Schwartz et al.*, 1983]. Incident solar wind ions simply reverse their component of velocity parallel to the shock normal [*Thomsen et al.*, 1983b]. In this case the postencounter parallel velocity in the plasma reference frame (normalized to v_{sw}) is given by,

$$P_{s.r.} = 2\cos(\theta_{Vn})\cos(\theta_{Bn}) \tag{8}$$

Table 3 summarizes the numerical values for each emission mechanism for each interval in θ_{Bx}.

The third column in Table 2 lists the numerical values of the normalized velocity P in the rest frame of an ion propagating along the UWFB. P is directly related to the slope of the boundary [*Meziane and D'Uston*, 1998]. This last value is compared to the normalized shock speed P_s given in the last column of Table 2. Table 3 clearly indicates that the ions propagating along the boundary are fast enough to escape upstream ($P \geq P_s$ for all θ_{Bx} values). The numerical values of P and P_s also indicate that the observations are in very good agreement with the magnetosheath leakage model only for $\theta_{Bx} = 45°$ and $\theta_{Bx} = 55°$ cases. On the other hand, the specular reflection model seems to be a weak model. This strongly suggests that backstreaming gyrating ion distributions resulting from specular reflection are not likely a source for wave excitation, a result which is consistent with previous studies [*Mazelle et al.*, 2003]. *Kucharek et al.* [2004] reported strong observational evidence that magnetosheath leakage is not a source mechanism for FAB production. To overcome the problem of the injection, *Kucharek et al.* [2004] proposed that FABs may result from pitch angle scattering of specularly reflected ions (which could occur for all shock geometries). The ions with high parallel speed would escape upstream and the resulting particle distribution would then appear as FABs. The obtained parallel speed by *Kucharek et al.* [2004] (which results after the pitch angle scattering) is equal to the one obtained directly from a direct reflection with conservation of the magnetic moment. Therefore, equation (7) used in the present paper could correspond to either an adiabatic reflection or to the mechanism described in *Kucharek et al.* [2004]. However, the boundary-derived velocity is underestimated compared to the one obtained from the adiabatic reflection hypothesis.

7. Conclusions

Using a well-defined, accurate, and robust criterion, we present a new determination of the boundary for ULF waves in the Earth foreshock (which we termed UWFB). Our criterion allows to quantitatively measure differences between the magnetic field upstream and downstream from the UWFB, taking into account possible rotations of the IMF.

All the wave events reported in the present paper show evidence of magnetic connectivity to the Earth bow shock models, which is a clear indication that these waves are associated with the Earth foreshock. As mentioned in section 3, the precise location of the UWFB is only determined under quasi-stationary IMF conditions. The foreshock geometry critically depends on the IMF direction. The standard picture to explain the origin of the ULF foreshock, assumes a stationary IMF and ion beams generated (by different theoretical mechanisms)

at the bow shock and backstreaming along magnetic field lines. These beams traveling along stationary field lines are the ultimate cause of ULF waves that, once generated, propagate downstream. Within this general framework, the main purpose of our study is to identify the location of the ULF foreshock boundary under conditions that can be regarded as (at least approximately) stationary. Therefore, assuming that the overall foreshock structure remains in a stationary regime, the crossing of the UWFB corresponds to rather mild rotations of the IMF (i.e., small values of α). Based on our statistical study of the α angle, we assume that Cluster crosses the quasi-stationary UWFB whenever $\alpha < 12.5°$. We choose this limiting angle because we consider that this value is sufficiently small and yet it allows for a substantial number of crossings. On the other hand, relatively large values of α correspond to nonstationary configurations, and therefore, we filter these cases out, since the boundary in these cases is also nonstationary.

For $\theta_{Bx} = 45°$ the boundary forms an angle of $87° \pm 6°$ with respect to the $\hat{\mathbf{x}}_{GSE}$. The observed UWFB is located downstream with respect to the predicted theoretical boundary (78°), in agreement with the theoretical prediction [*Skadron et al.*, 1988]. We speculate that this difference might be due to the fact that *Skadron et al.* [1988] criterion is based on the compressive component of the fluctuations, where the amplitude of the waves may be smaller than the ones that we observe.

Throughout the UWFB a transition take place from FAB distributions (without the presence of ULF waves) to gyrating ion distributions (with the occurrence of ULF waves). However, if we consider the *Bonifazi and Moreno* [1981a] classification, our statistical boundary is compatible with the presence of diffuse distributions in the downstream region. We emphasize that the large spread and lack of consideration of the IMF cone in the classification performed by *Bonifazi and Moreno* [1981a] stem from the fact that these determinations are contaminated from several ions distributions. On other hand, our statistical results are in agreement with the UWFB reported by GB86 and the ion foreshock boundary presented by MD98. However, we note that the correlation between waves and the presence of some type of ion distributions is strongly dependent on the mechanism of generation of the ULF waves. Therefore, it is necessary to pursue a detailed investigation of the ion distribution function at both sides of the UWFB to infer any kind of correlation between ion distributions and waves.

To understand the variation of the boundary with the cone angle θ_{Bx}, we examined the speed of ions propagating along this boundary and compared the obtained results with the classical mechanisms. We have found that the specularly reflected ions are excluded in providing the necessary energy for the wave excitation. Moreover, the hypothesis of adiabatic reflection predicts ion speeds that are larger than those associated with the UWFB. One possible explanation for this behavior is suggested: that the difference may be due to momentum exchange between the incident solar wind population and the backstreaming particles through the wave-particle interaction resulting from a beam-plasma instability.

A comprehensive understanding of the UWFB in the context of the wave-particle interaction requires the detailed study of the ion distribution function of each for the 102 crossings at both sides of the UWFB boundary to conclude which type of ion distributions are present. This will be the scope of a future work.

References

Andrés, N., D. O. Gómez, C. Bertucci, C. Mazelle, and M. K. Dougherty (2013), Saturn's ULF wave foreshock boundary: Cassini observations, *Planet. Space Sci.*, *79–80*, 64–75.

Asbridge, J. R., S. J. Bame, and I. B. Strong (1968), Outward flow of protons from the Earth's bow shock, *J. Geophys. Res.*, *73*, 5777–5782.

Balogh, A., et al. (1997), The Cluster magnetic field investigation, *Space Sci. Rev.*, *79*, 65–91.

Binsack, J. H., and V. M. Vasyliunas (1968), Simultaneous IMP 2 and OGO 1 observations of bow shock compression, *J. Geophys. Res.*, *73*, 429–433.

Bonifazi, C., and G. Moreno (1981a), Reflected and diffuse ions backstreaming from the Earth's bow shock. 1: Basic properties, *J. Geophys. Res.*, *86*, 4397–4413.

Bonifazi, C., and G. Moreno (1981b), Reflected and diffuse ions backstreaming from the Earth's bow shock. 2: Origin, *J. Geophys. Res.*, *86*, 4405–4414.

Burgess, D., et al. (2005), Quasi-parallel shock structure and processes, *Space Sci. Rev.*, *118*(1–4), 205–222.

Convery, P. D., and S. P. Gary (1997), Electromagnetic proton cyclotron ring instability: Threshold and saturation, *J. Geophys. Res.*, *102*, 2351–2358.

Diodato, L., E. W. Greenstadt, G. Moreno, and V. Formisano (1976), A statistical study of the upstream wave boundary outside the Earth's bow shock, *J. Geophys. Res.*, *81*(1), 199–204.

Eastwood, J. P., A. Balogh, E. A. Lucek, C. Mazelle, and I. Dandouras (2003), On the existence of Alfvén waves in the Terrestrial foreshock, *Ann. Geophys.*, *21*, 1457–1465.

Eastwood, J. P., E. A. Lucek, C. Mazelle, K. Meziane, Y. Narita, J. Pickett, and R. A. Treumann (2005), The foreshock, *Space Sci. Rev.*, *118*, 41–94.

Edmiston, J. P., C. F. Kennel, and D. Eichler (1982), Escape of heated ions upstream of quasi-parallel shocks, *Geophys. Res. Lett.*, *9*, 531–534.

Fairfield, D. H. (1969), Bow shock associated waves observed in the far upstream interplanetary medium, *J. Geophys. Res.*, *74*, 3541.

Farris, M. H., S. M. Petrinec, and C. T. Russell (1991), The thickness of the magnetosheath: Constraints on the polytropic index, *Geophys. Res. Lett.*, *18*(10), 1821–1824.

Fazakerley, A. N., A. J. Coates, and M. W. Dunlop (1995), Observations of upstream ions, solar wind ions and electromagnetic waves in the Earth's foreshock, *Adv. Space Res.*, *15*, 103–106.

Fuselier, S., M. Thomsen, S. Gary, S. Bame, C. Russell, and G. Parks (1986b), The phase relationship between gyrophase-bunched ions and MHD-like waves, *Geophys. Res. Lett.*, *13*, 60–63.

Fuselier, S. A. (1994), Suprathermal ion upstream and downstream from the Earth's bow shock, in *Solar Wind Sources of Magnetospheric Ultra-Low-Frequency Waves, Geophys. Monogr. Ser.*, vol. 84, edited by M. J. Engebretson, K. Takahashi, and M. Scholer, pp. 107–119, AGU, Washington, D. C.

Fuselier, S. A., M. F. Thomsen, J. T. Gosling, S. J. Bame, and C. T. Russell (1986a), Gyrating and intermediate ion distributions upstream from the Earth's bow shock, *J. Geophys. Res.*, *91*, 91–99.

Gary, S. P. (1991), Electromagnetic ion/ion instabilities and their consequences in space plasmas: A review, *Space Sci. Rev.*, *56*, 373–415.

Gary, S. P. (1993), *Theory of Plasma Microestabilities*, Cambridge Univ. Press, New York.

Gosling, J. T., J. R. Asbridge, S. J. Bame, G. Paschmann, and N. Sckopke (1978), Observations of two distinct populations of bow shock ions in the upstream solar wind, *Geophys. Res. Lett.*, *5*, 957–960.

Gosling, J. T., M. F. Thomsen, S. J. Bame, W. C. Feldman, G. Paschmann, and N. Sckopke (1982), Evidence for specularly reflected ions upstream from the quasi-parallel bow shock, *Geophys. Res. Lett.*, *9*(12), 1333–1336.

Gosling, J. T., M. F. Thomsen, S. J. Bame, and C. T. Russell (1989), On the source of diffuse, suprathermal ions observed in the vicinity of the Earth's bow shock, *J. Geophys. Res.*, *94*, 3555–3563.

Greenstadt, E., and L. Baum (1986), Earth's compressional foreshock boundary revisited: Observations by the ISEE 1 magnetometer, *J. Geophys. Res.*, *91*(A08), 9001–9006.

Greenstadt, E., G. Le, and R. J. Strangeway (1995), ULF waves in the foreshock, *Adv. Space Res.*, *15*, 71–84.

Gurgiolo, C., G. K. Parks, and B. H. Mauk (1983), Upstream gyrophase bunched ions: A mechanism for creation at the bow shock and the growth of velocity space structure through gyrophase mixing, *J. Geophys. Res.*, *88*(11), 9093–9100.

Hoppe, M. M., and C. T. Russell (1983), Plasma rest frame frequencies and polarizations of the low-frequency upstream waves: ISEE 1 and 2 observations, *J. Geophys. Res.*, *88*, 2021–2028.

Hoppe, M. M., C. T. Russell, L. A. Frank, T. E. Eastman, and E. W. Greenstadt (1981), Upstream hydromagnetic waves and their association with backstreaming ion populations: ISEE 1 and 2 observations, *J. Geophys. Res.*, *86*, 4471–4492.

Hoshino, M., and T. Terasawa (1985), Numerical study of the upstream wave excitation mechanism. Nonlinear phase bunching of beam ions, *J. Geophys. Res.*, *90*(1), 57–64.

Jones, F. C., and D. C. Ellison (1991), The plasma physics of shock acceleration, *Space Sci. Rev.*, *58*, 259–346.

Kucharek, H., E. Möbius, M. Schöler, C. Mouikis, L. Kistler, T. Horbury, A. Balogh, H. Réme, and J. Bosqued (2004), On the origin of field-aligned beams at the quasi-perpendicular bow shock: Multi-spacecraft observations by Cluster, *Ann. Geophys.*, *22*, 2301–2308.

Le, G., and C. T. Russell (1992a), A study of ULF wave foreshock morphology—II: Spatial variation of ULF waves, *Planet. Space Sci.*, *40*(9), 1215–1225.

Le, G., and C. T. Russell (1992b), A study of ULF wave foreshock morphology—I: ULF foreshock boundary, *Planet. Space Sci.*, *40*(9), 1203–1213.

Lin, R. P., C. I. Meng, and K. A. Anderson (1974), 30- to 100-kev protons upstream from the Earth's bow shock, *J. Geophys. Res.*, *79*, 489–498.

Lucek, E. A., T. S. Horbury, M. W. Dunlop, P. J. Cargill, S. J. Schwartz, A. Balogh, P. Brown, C. Carr, K. H. Fornacon, and E. Georgescu (2002), Cluster magnetic field observations at a quasi-parallel bow shock, *Ann. Geophys.*, *20*, 1699–1710.

Mazelle, C., D. Le Quéau, and K. Meziane (2000), Nonlinear wave-particle interaction upstream from the Earth's bow shock, *Nonlinear Processes Geophys.*, *77*, 185–190.

Mazelle, C., et al. (2003), Production of gyrating ions from nonlinear wave-particle interaction upstream from the Earth's bow shock: A case study from Cluster-CIS, *Planet. Space Sci.*, *51*, 785–795.

Merka, J., A. Szabo, J. A. Slavin, and M. Peredo (2005), Three-dimensional position and shape of the bow shock and their variation with upstream mach numbers and interplanetary magnetic field orientation, *J. Geophys. Res.*, *110*, A04202, doi:10.1029/2004JA010944.

Meziane, K., and C. D'Uston (1998), A statistical study of the upstream intermediate ion boundary in the Earth's foreshock, *Ann. Geophys.*, *16*, 125–133.

Meziane, K., et al. (1997), Wind observation of gyrating-like ion distributions and low frequency waves upstream from the Earth's bow shock, *Adv. Space. Res.*, *20*, 703–706.

Meziane, K., C. Mazelle, R. P. Lin, D. LeQuéau, D. E. Larson, G. K. Parks, and R. P. Lepping (2001), Three-dimensional observations of gyrating ion distributions far upstream from the Earth's bow shock and their association with low-frequency waves, *J. Geophys. Res.*, *106*(A4), 5731–5742.

Meziane, K., et al. (2004a), Bow shock specularly reflected ions in the presence of low-frequency electromagnetic waves: A case study, *Ann. Geophys.*, *22*, 2325–2335.

Meziane, K., et al. (2004b), Simultaneous observations of field-aligned beams and gyrating ions in the Terrestrial foreshock, *J. Geophys. Res.*, *109*, A05107, doi:10.1029/2003JA010374.

Meziane, K., A. M. Hamza, M. Wilber, C. Mazelle, and M. A. Lee (2013), On the field-aligned beam thermal energy, *J. Geophys. Res. Space Physics*, *118*, 6946–6954, doi:10.1002/2013JA019060.

Miao, B., H. Kucharek, E. Möbius, C. Mouikis, H. Matsui, Y. C.-M. Liu, and E. A. Lucek (2009), Remote sensing of local structure of the quasi-perpendicular Earth's bow shock by using field-aligned beams, *Ann. Geophys.*, *27*(3), 913–921.

Möbius, E., et al. (2001), Observations of the spatial and temporal structure of field-aligned beam and gyrating ring distributions at the quasi-perpendicular bow shock with Cluster cis, *Ann. Geophys.*, *19*, 1411–1420.

Paschmann, G., N. Sckopke, S. J. Bame, J. R. Asbridge, C. T. Russell, and E. W. Greenstadt (1979), Association of low-frequency waves with suprathermal ions in the upstream solar wind, *Geophys. Res. Lett.*, *6*, 209–212.

Paschmann, G., N. Sckopke, I. Papamastorakis, J. R. Asbridge, S. J. Bame, and J. T. Gosling (1981), Characteristics of reflected and diffuse ions upstream from the Earth's bow shock, *J. Geophys. Res.*, *86*, 4355–4364.

Réme, H., et al. (2001), First multispacecraft ion measurements in and near the Earth's magnetosphere with the identical Cluster ion spectrometry (CIS) experiment, *Ann. Geophys.*, *19*, 1303–1354.

Sarris, E. T., G. C. Anagnostopoulos, and S. M. Krimigis (1987), Simultaneous measurements of energetic ion (50 keV and above) and electron (220 keV and above) activity upstream of Earth's bow shock and inside the plasma sheet—Magnetospheric source for the November 3 and December 3, 1977 upstream events, *J. Geophys. Res.*, *92*, 12,083–12,096.

Savoini, P., B. Lembege, and J. Stienlet (2013), On the origin of the quasi-perpendicular ion foreshock: Full-particle simulations, *J. Geophys. Res.*, *118*, 1132–1145.

Schöler, M., H. Kucharek, and J. Giacalone (2000), Cross-field diffusion of charged particles and the problem of ion injection and acceleration at quasi-perpendicular shocks, *J. Geophys. Res.*, *105*(A8), 18,285–18,293.

Schwartz, S. J., M. F. Thomsen, and J. T. Gosling (1983), Ions upstream of the Earth's bow shock: A theoretical comparison of alternative source populations, *J. Geophys. Res.*, *88*(A03), 2039–2047.

Skadron, G., R. D. Holdaway, and M. A. Lee (1988), Formation of the wave compressional boundary in the Earth's foreshock, *J. Geophys. Res.*, *93*, 11,354–11,362.

Sonnerup, B. U. O. (1969), Acceleration of particles reflected at a shock front, *J. Geophys. Res.*, *74*(5), 1301–1304.

Tanaka, M., C. C. Goodrich, D. Winske, and K. Papadopoulos (1983), A source of the backstreaming ion beams in the foreshock region, *J. Geophys. Res.*, *88*, 3046–3054.

Thomsen, M. F., J. T. Gosling, S. J. Bame, W. C. Feldman, G. Paschmann, and N. Sckopke (1983a), Field-aligned ion beams upstream of the earth's bow shock: Evidence for a magnetosheath source, *Geophys. Res. Lett.*, *10*, 1207–1210.

Thomsen, M. F., S. J. Schwartz, and J. T. Gosling (1983b), Observational evidence on the origin of ions upstream of the Earth's bow shock, *J. Geophys. Res.*, *88*, 7843–7852.

Thomsen, M. F., J. T. Gosling, S. J. Bame, and C. T. Russell (1985), Gyrating ions and large-amplitude monochromatic MHD waves upstream of the Earth's bow shock, *J. Geophys. Res.*, *90*, 267–273.